Groundwater risk intensity mapping in semi-arid regions using optical remote sensing data as an additional tool

Heike Werz · Heinz Hötzl

Abstract Due to semi-arid to arid climatic conditions, Jordan has limited groundwater resources. As a result of agricultural activities and untreated wastewater, most of the groundwater in the karstic areas is microbiologically contaminated. Groundwater vulnerability, hazards, and risk intensity were mapped (scale 1:50,000) at a test site near the Jordan Rift Valley. The mapping included the use of optical remote sensing to complement conventional data in areas with poor data. LANDSAT ETM+ data, and colour and panchromatic aerial photographs at different scales were incorporated using visual image interpretation and digital image processing. The applicability of the different remote sensing data sources is discussed and recommendations for their usage are given. Information derived from digital images offers new opportunities for vulnerability and hazard assessment, particularly when related to land use, vegetation cover, urbanisation and infrastructure. The resulting maps indicate clearly the vulnerable areas and the "hot spots" of potential contamination in the test site and form an important basis for integrated groundwater management studies and the long-term planning of protective measures. The application and transferability of the European vulnerability approach (COST Action 620) to the test site in Jordan proved to be good, in general, although modifications were necessary to suit local conditions.

Résumé La Jordanie ne dispose que de ressources limitées en eaux souterraines, étant donné le climat semi-aride à aride prévalant dans ce pays. La contamination microbiologique de la plupart des eaux souterraines des régions karstiques est due aux activités agricoles et l'absence de traitement des eaux usées. La vulnérabilité des eaux souterraines, et le danger et l'intensité du risque de leur contamination ont été cartographiés (à l'échelle de 1:50 000) pour un site d'étude situé près de la vallée du Rift du Jourdain. La cartographie inclut l'utilisation de données optiques de télédétection pour complémenter les sources de données conventionnelles, dans les zones où la couverture est déficiente. Des données de LANDSAT ETM+ et des photographies aériennes en couleur et panchromatiques à différentes échelles ont été incorporées en utilisant des méthodes d'interprétation visuelle et informatique de l'image. La qualité des différentes sources de données de télédétection est discutée et évaluée, et des recommandations pour leur utilisation sont suggérées. L'informations obtenue des images digitales offre de nouvelles opportunités pour l'évaluation des vulnérabilités et des dangers, surtout reliés à l'usage du sol, la couverture végétale, l'urbanisation et les diverses infrastructures. Les cartes ainsi obtenues indiquent clairement les zones vulnérables et les points critiques potentiels pour la contamination du site d'étude et forment une base importante pour l'étude de la gestion intégrée des eaux souterraines et pour la planification à long terme des mesures de protection. L'applicabilité de l'approche européenne de cartographie de la vulnérabilité et des risques (COST action 620) au site d'étude jordanien est généralement approprié, même si certaines modifications ont été nécessaires pour s'ajuster aux particularités régionales.

Resumen Los recursos hídricos subterráneos en Jordania son limitados debido principalmente a su clima semi árido. En la mayoría de las áreas kársticas, las aguas subterráneas están contaminadas microbiológicamente a consecuencia de la actividad agrícola y de las aguas residuales. Por ello, se han realizado mapas de peligro, vulnerabilidad e intensidad del riesgo (a escala 1/50.000) de un área piloto próxima al Rift en Jordania. Los mapas han sido elaborados con el apoyo de técnicas de teledetección en aquellas zonas donde la información era escasa. Se han utilizado imágenes del LANDSAT ETM+ a y fotografía aérea, de color y pancromática, a diferentes escalas para el procesamiento de las imágenes digitales y la fotointerpretación. En este trabajo se discute y se dan recomendaciones sobre la aplicabilidad

Received: 19 July 2005 / Accepted: 13 June 2007
Published online: 20 July 2007

Electronic supplementary material The online version of this article (doi:10.1007/s10040-007-0202-0) contains supplementary material, which is available to authorised users.

H. Werz (✉) · H. Hötzl
Department of Applied Geology, Hydrogeology,
University of Karlsruhe,
Kaiserstrasse 12,
76128 Karlsruhe, Germany
e-mail: werz@agk.uka.de

H. Hötzl
e-mail: hoetzl@agk.uka.de

 DOI 10.1007/s10040-007-0202-0

de las diferentes imágenes de satélite en los análisis de teledetección. Los datos que se pueden derivar de las imágenes digitales son un avance para la evaluación de la vulnerabilidad y los peligros de contaminación, particularmente aquellos referidos a usos del suelos, cubierta vegetal e infraestructuras urbanas. Los mapas resultantes muestran claramente la vulnerabilidad y los peligros potenciales de contaminación en la zona de estudio, lo que genera una importante base para los estudios de gestión integrada de las aguas subterráneas y de planificación de las medidas protectoras. La aplicabilidad de la aproximación europea a los estudios de vulnerabilidad en karst (COST Action 620) en la zona de estudio (Jordania) es buena, aunque fueron necesarias algunas leves modificaciones de la metodología para ajustarla a las condiciones locales.

Keywords Vulnerability mapping · Hazards mapping · Groundwater protection · Remote sensing · Jordan

Introduction

At present, Jordan is overusing all of its annual renewable groundwater resources, leading to a degradation of water quality and the abandonment of many wells (Chebaane et al 2004, Al-Kharabsheh-Atef 1999). Middle East experts agree that it is not only the water quantity but also the degradation of its quality that endangers the future use of the limited groundwater resources (Dottridge and Jaber-Abu-Nizar 1999, Salameh 1996). Water quality is endangered by salinisation and contamination, mainly caused by agro-chemicals and microbiological substances (Al-Farajat 2001). Because of the need to improve the environmental situation, a first step that is proposed is to define groundwater protection areas using groundwater vulnerability, hazard- and groundwater-risk intensity maps. This will be one of the basic tools for integrated groundwater management strategies in the region.

The term “groundwater vulnerability” is used to define the sensitivity of groundwater to contaminants. The concept of groundwater vulnerability is based on the assumption that the physical environment provides natural protection to groundwater against contaminants resulting from human impact entering the subsurface environment (Vrba and Zaporozec 1994). The European Union’s COST Action 620 on “Vulnerability mapping for the protection of carbonate (karst) aquifers”, defines “groundwater hazards” as potential sources of contamination resulting from human activities taking place mainly at the land surface (De Katelaere et al. 2004). “Risk intensity” reflects the probability of groundwater to be actually contaminated by human activities showing that the highest risk of contamination exists where a dangerous hazard is located in zones that are characterised by highly vulnerable aquifers.

The construction of groundwater vulnerability and hazard maps is often confronted with insufficient topographical, hydrological, and hydrogeological data. Therefore, the main emphasis at the test site was to produce actual digital topographic map information using remote sensing data as an additional data source that can be used as a basic parameter for vulnerability and hazard assessment. High-resolution digitised colour aerial photographs were used for a section of the test site to assess the degree of karstification and for the identification and location of point-source hazards. The integrated approach of using remote-sensing data in conjunction with geographic information system (GIS) techniques is a helpful tool in solving the problem of insufficient data.

In this paper, an overview of existing approaches that use remote-sensing techniques in groundwater vulnerability and hazard mapping is included, followed by a description of the processed remote sensing data sets, and of the generation of the vulnerability-, hazard- and risk-intensity maps. Finally, the usefulness of optical remote sensing data and the applicability and transferability of the European vulnerability-, hazard- and risk-intensity approaches to the test site in Jordan is discussed and an outlook for an improved groundwater management of the test site is given.

Existing studies of groundwater contamination and hazard mapping using remote sensing data

Groundwater vulnerability assessments using land-use data based on satellite images were carried out by Magiera (2002), Al-Adamat et al. (2003), Bressan and Dos Anjos (2003), but in many studies the use of remote sensing data for vulnerability assessment is proposed theoretically without going into detail or presenting practical applications (Spiteri 2004, Margane 2002). The main difference between the Cost Action 620 hazard inventory and existing approaches for hazard assessment is that the hazard maps are limited to “potential” hazards caused by human activities that pose a potential polluting activity, and can potentially have an impact on groundwater. Existing approaches of hazard mapping do not generally map locations and places where potential hazards can be released. Instead they assess existing hazards that have already contaminated the environment in some way, and show visible or measurable consequences on the water quality, or changes in vegetation pattern and growth of plants.

In this context, several previous studies deal with the monitoring of water quality, wastewater effluents, non-point source pollution, and hazardous waste sites using remote sensing data (Schultz and Engman 2000, Engman and Gurney 1991, Dekker et al. 1995, Finkbeiner and O’Tool 1985, Farrell 1985, Svoma and Pysek 1985).

Surface-water quality parameters have successfully been monitored in the open ocean and in large lakes using optical multispectral and hyperspectral remote sensing data, including sediments (suspended solids), algae (chlorophyll), gelbstoffe (dissolved organic compounds) and Secchi disk transparency (Koponen et al. 2002, Thiemann and Kaufmann 2002, Härmä et al. 2001, Bukata et al. 1991, Hudson et al. 1994). Ultraviolet

 DOI 10.1007/s10040-007-0202-0

photography was used for mapping oil spills on surface water bodies; while thermal infrared was used for detection of seepage from leach fields and underground storage tanks. Remote sensing studies, including techniques such as low frequency airborne electromagnetic methods (AEM), were used for the detection of variations in groundwater salinity and deeper brine contaminated aquifers (D'Sa et al. 2000, Srivastava et al. 1997, Ellyett and Pratt 1975). Farrell (1985) evaluated colour infrared photographs for the identification of onsite wastewater soil absorption systems. Contamination of groundwater was studied by Svoma (1985) using colour and colour infrared aerial photographs for detection of changes in vegetation, and for detecting groundwater pollution by industrial fertilizers, oil leaks, and natural gas leaks, after actual emergencies and on experimental sites. Mattikalli and Engman (2000) used agricultural non-point source pollution models that estimate nitrogen, phosphorus and chemical oxygen demand concentration in runoff. Such models assess agricultural impact on surface water quality based on controlling parameters including land cover, land use, soils and topography. Non-point source-pollution modeling using remote sensing data was done by Chowdary et al. (2004), Davenport et al. (2003), Basnyat et al. (2000), Kim and Ventura (1993), Ragan and Rogers (1978), Schecter (1976), OKI (1975).

Most studies of groundwater hazard assessment produce qualitative or semi-quantitative results; often remote sensing data is only used indirectly to assess the needed parameters. The use of data from a particular image is limited to the particular conditions in a relatively small test site, a plant species, or in a special hydrogeological situation. Such data cannot be transferred or applied to other areas; nor can it be used for regional investigations of groundwater zones in areas with near-surface groundwater occurrences. In the case of a thick unsaturated zone of a karstic aquifer, the plants are independent of the groundwater level, and the roots are not in contact with the contaminated water and thus cannot be used as an indicator for groundwater contamination.

Test site

The test site is located in Jordan on the western slopes of the eastern highlands of the Jordan Rift Valley, about 20 km northeast of the Dead Sea (Fig. 1). The geographical borders of the test site coincide with the surface catchment area of the main wadi, Wadi Shu'ayb. The area, with a total size of 185 km^2, is topographically complex and characterised by a steep relief, with elevations ranging from −200 m in the southwest up to 1,240 m above sea level (m asl) in the northeast. The semi-arid climate of the test site belongs to the Mediterranean climate zone, with large seasonal and daily temperature variations (Bender 1974). Daily average temperatures vary from 10 to 30°C. During

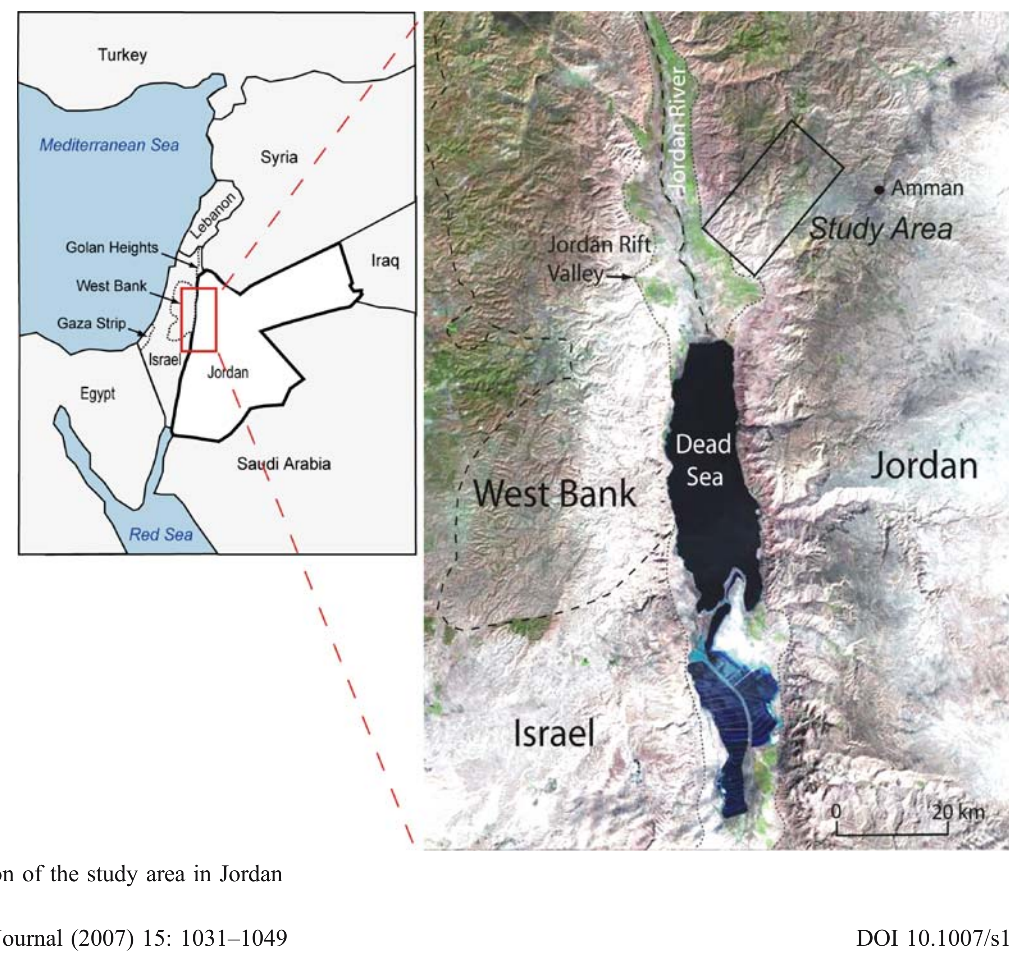

Fig. 1 Location of the study area in Jordan

DOI 10.1007/s10040-007-0202-0

the one rainy season between November and March, precipitation ranges from less then 150 mm/year in the southern part to 600 mm/year in the high-elevated northern parts. Due to high-evaporation rates, only approximately 12% of the precipitation infiltrates into the aquifer and contributes to groundwater recharge (Ta′any 1992).

Land cover and land use of the area vary due to variations in the climate and elevation. Wherever possible, the middle and northern parts of the test site are used for agricultural purposes. Urban centres and industrial areas are located only in the northern and northeastern areas, whereas low population densities characterize the southern parts of the test site.

The SW border of the test site is situated at the transition zone between the Jordan Rift Valley and the eastern highlands. The area is dominated by sedimentary rocks of Upper Cretaceous Age (Albian to Maastrichtian), mainly limestones, dolomites and marls of the Ajlun and Belqa Groups which are underlined by Kurnub sandstones of the Lower Cretaceous age, with outcrops on fault zones along the so-called Wadi Shu’ayb structure, which will be described later (Mikbel and Zacher 1981, Salameh 1980, Bender 1974). The Ajlun Group consists of approximately 350–400 m thick interbedded karstic limestone, marly limestone and dolomitic limestone. Figure 2 shows the stratigraphy of the test site based on Masri (1963) and Quennel (1951).

The Belqa Group includes a sequence of mainly limestone intercalated with thick-bedded chert, but also chalk, marls, silicified limestone and phosphatic horizons. The test site is extensively crossed by normal faults of variable throws and trends and by several anticlines and synclines. The prevailing fault directions are NW–SE and NNE–SSW (Fig. 3). The dominating structural element is the Wadi Shu’ayb structure, a fold belt of approximately 25 km length and 1–4 km width which extends from the south near Shunat Nimrin in a northeasterly direction (Mikbel and Zacher 1981) and continues into the Suweilih structure located northeast of the test site (Salameh 1980).

Two main aquifer complexes can be distinguished in the test site: the Lower and the Upper Cretaceous Aquifer complexes. The latter is the more important one, and includes the complete sequence of the Ajlun Group (Fig. 2). Three subaquifers are relevant for the area within the Ajlun Group: the Na’ur Aquifer (A1/2); the Hummar Aquifer (A4); and the Wadi as Sir Aquifer (A7). These subaquifers are drained by several springs that are partly used to supply drinking water. The aquifers are interbedded with the Fuheis (A3) and the Shu’ayb (A5/6) formations, which are both composed of interlaid thin layers of marls, dolomitic thinly bedded limestone, or siltstone and act as leaking aquitards. The subaquifers are connected through fractures and broad fault zones, especially in tectonic compressive areas within the test site. The Lower Aquifer Complex in the test site is only represented by a small outcrop of the coloured sandstones of the Kurnub Group along the Wadi Shu’ayb structure. No significant springs emerge from the Lower Aquifer Complex.

Data sources and preprocessing

LANDSAT ETM$^+$ data

The LANDSAT 7 Enhanced Thematic Mapper Plus (ETM$^+$) is a NASA (US National Aeronautics and Space Administration) Earth resource satellite that acquires

Period	Epoch	Group	Formation	Symbol	Brief description	Thick-ness
		Quennel Group (1951)	Masri (1963)			
Upper Cretaceous	Campanian Santonian Coniasian	Belqa	Amman al Hisa	B2	Phosphorite and silicified limestone	~ ?? m
			Wadi Um Ghudran	B1	Chalk, marl, fossiliferous	~ 10 m
	Turonian	Ajlun	Wadi as Sir	A7	Thin layered dolomite or massive limestone, fossiliferous, chert layers, karstified	~ 130 m
	Cenomanian		Wadi Shuayb	A5/6	Limestone (A6), thin layered limestone and marl (A5)	~ 30 m
			Hummar	A4	Massive limestone, often karstified, dolomite	~ 45m
			Fuheis	A3	Thin layered limestone, marl	~ 70 m
			Naur	A1/2	Massive limestone, chert layers (A2), marl (A1)	~ 110 m
Lower Cretaceous	Albian	Kurnub	Subeihi	K2	Multicolour sandstone	~ 250 m
	Abtian Neocomian		Aardo	K1	White, yellow massive sandstone	

Fig. 2 Stratigraphy in the test site (modified after Powell 1989)

DOI 10.1007/s10040-007-0202-0

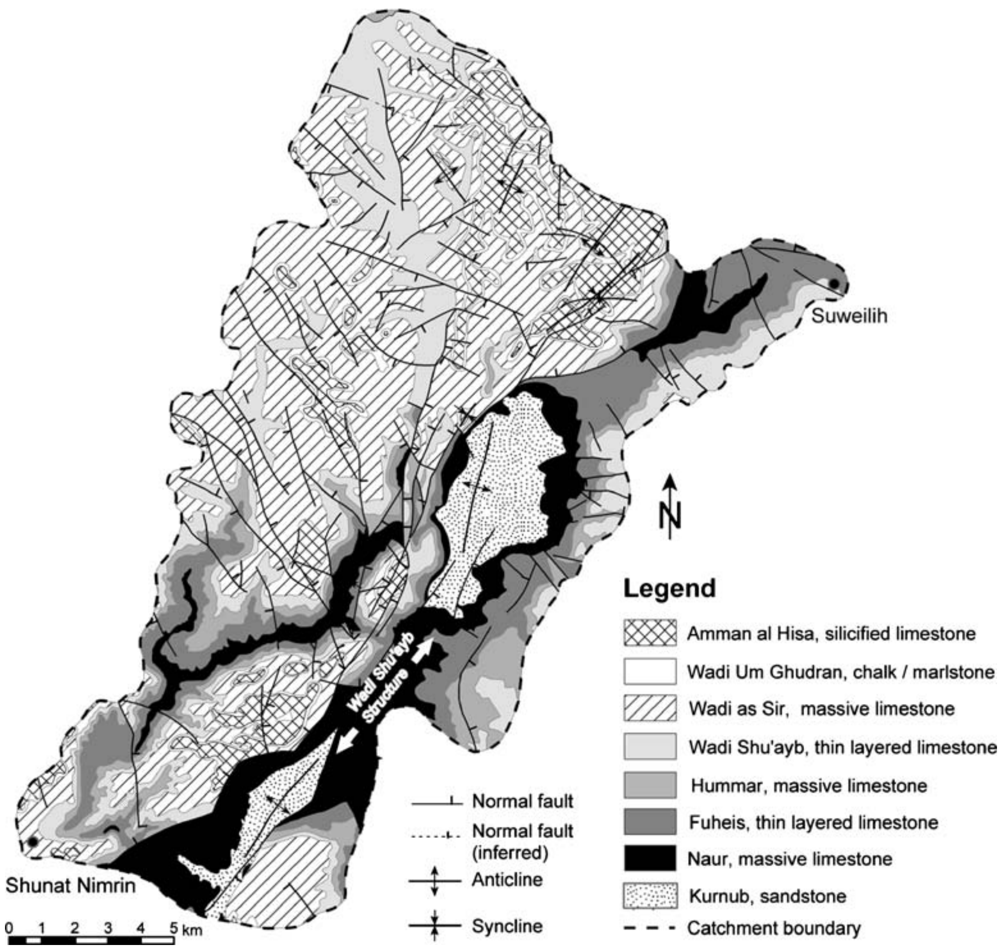

Fig. 3 Geological map of the study area

multispectral images in six bands of data in the visible (0.45–0.69 μm), near-infra-red (IR) (0.76–0.90 μm), and mid-IR (1.55–1.75 and 2.08–2.35 μm) spectral regions at resolutions of 30 m, 15 m for one resolution panchromatic band, and 60 m for one thermal band (10.4–12.5 μm). LANDSAT ETM$^+$ imagery was chosen because it combines extensive geographical coverage, wide spectral range, good vegetation discrimination, very good data availability and is relatively cost-effective as compared to conventional data collection. Unfortunately, since early June 2003, a permanent mechanical failure of onboard electronics has caused information gaps in LANDSAT ETM$^+$ data.

Georeferencing, geocoding, linear contrast stretching and pan-sharpening were applied to preprocess the image. The data were classified by applying unsupervised and supervised image classification algorithms for land cover and land use. For the unsupervised classification, the ISODATA (iterative self-organising data analysis) technique was chosen. The information classes for the supervised classification were defined by visual inspection of the false colour composites RGB (red green blue)=432 and RGB=541 of the LANDSAT ETM$^+$ image and from topographic maps, panchromatic aerial photographs, digital colour photographs, and results from a first field survey. The supervised classification was applied using the Maximum Likelihood algorithm. Homogenous regions (as classified by the ISODATA algorithm), were examined for objects with known groundtruth reference and used as training areas. Additional global positioning system (GPS) groundtruth data were collected during detailed field work to be used at training sites.

The result of the supervised classification is shown in Fig. 4. Outcrops of naked or slightly overgrown limestone form a major part of the test site. The limestone is covered to varying degrees by soils and vegetation. A large part of the natural and anthropogenic influence on land surfaces in the test site appears relatively inhomogeneous. A complex mosaic of different structures forms each landscape unit. Particularly under the arid, but also under the semi-arid conditions, an area-wide soil or vegetation cover is missing and there is frequently only a patchy soil or vegetation cover. This pattern results in a high variability in the degree of land cover over short distances and thus in a high variability of the spectral composite of the pixels.

Furthermore, the different degree of irrigation or aridity of the plants leads to spectral differences within the same

 DOI 10.1007/s10040-007-0202-0

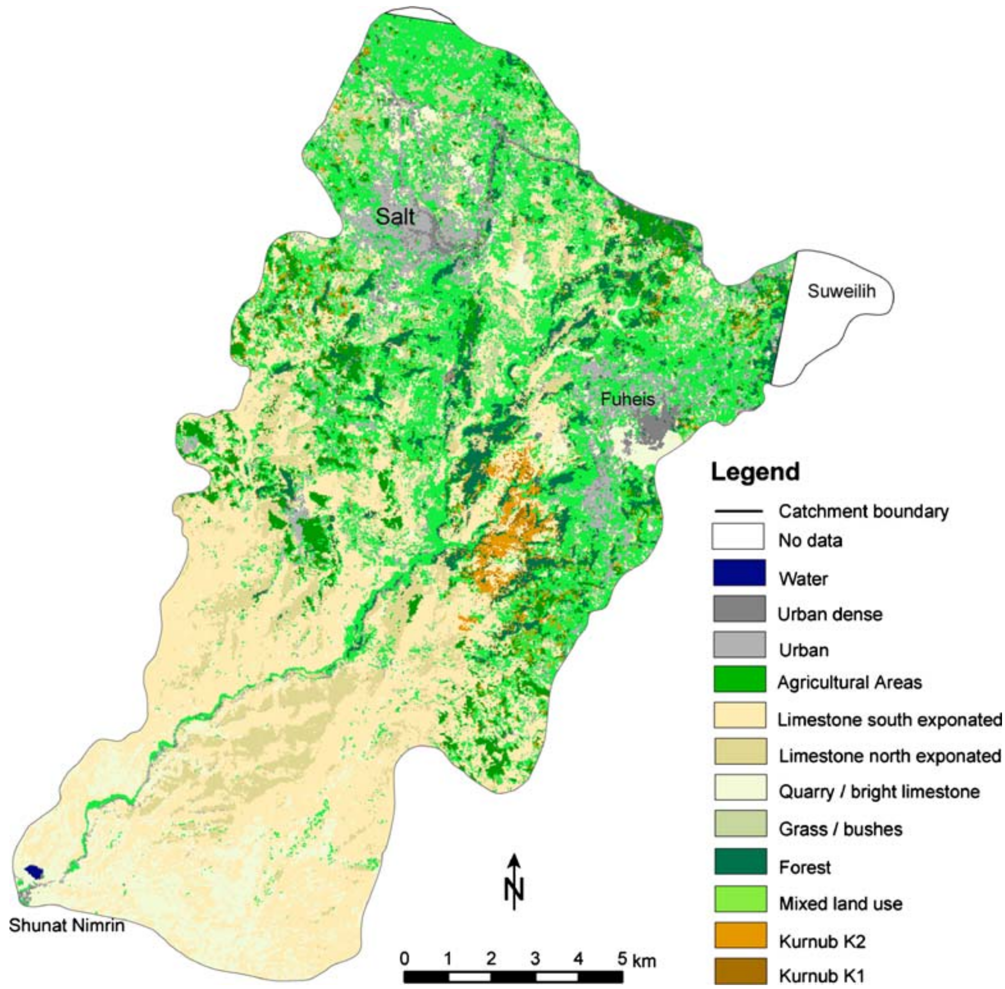

Fig. 4 Results of supervised classification of the LANDSAT ETM$^+$ subscene

information classes. Thus, mixed pixels present a difficult problem for the image classification of the test site. The very small size of individual fields with area equal or less than 900 m^2 (30×30 m, as determined by one ground cell of the multispectral LANDSAT ETM$^+$ bands) located between bushes and grass land, inevitably caused errors in the classification process. For the classification accuracy, 48 groundtruth areas (3,600 m^2) of representative and uniform land cover different from the training areas, were acquired and compared with the information classes obtained during the supervised classification. The confusion matrix of the supervised classification is shown in Table 1. The obtained classification accuracies, expressed as overall accuracy, producer's and user's accuracy, and the Kappa coefficient, are presented in Table 2.

The producer's accuracy indicates how well pixels of training sites of a given land-cover type are classified, whereas the user's accuracy specifies the probability that a pixel classified into a given category actually represents that category on the ground. The producer and user accuracies vary considerably between the information classes (Table 2). The classification accuracy mirrors the above-described conditions in the test site. Misclassifications occurred between mixed land use and agriculture areas and between Kurnub K2/K1 classes and the limestone north/south, due to similar spectral reflectance and due to the high variability of the pixel's spectral composite.

Analogue aerial photographs (1:30,000)

Paper prints of analogue black and white photographs with a film format of 23×23 cm (Wild RMK Top 15 camera) at a scale of 1:30,000 from October 1992 were used; more actual black and white photographs could not be made available. The photographs were scanned at a resolution of 16 lines per mm (lp/mm)—equivalent to 800 dots per inch (dpi)—with an office flat bed scanner corresponding to a ground cell size of 0.9 m. After the orthorectification process, all orthophotos were merged into a mosaic and loaded in ArcGIS. By on-screen digitising, thematic maps showing the infrastructure, urbanisation, crops, orchards, forest and drainage density were produced. The thematic maps were taken as inputs for the soil, land use and infiltration conditions for groundwater vulnerability and for hazard mapping.

 DOI 10.1007/s10040-007-0202-0

Table 1 Confusions matrix of the supervised classification of the LANDSAT ETM+ data. The numbers 1–12 refer correspond to the 12 classes

Classified data (in pixels)	Groundtruth (in pixels)												
Class[a]	1	2	3	4	5	6	7	8	9	10	11	12	Sum
1.Water	–	–	–	–	–	–	–	–	–	–	–	–	–
2. Urban (dense)	–	32	0	0	0	0	0	0	0	0	0	0	32
3. Urban	–	16	36	0	0	0	0	0	0	0	0	0	52
4. Agricultural areas	–	0	0	56	0	4	0	0	0	8	0	0	68
5. Limestone south	–	0	12	4	148	0	8	32	16	12	16	0	248
6. Limestone north	–	0	0	0	4	56	0	16	4	0	0	0	80
7. Quarry/bright limestone	–	0	0	0	0	16	40	0	0	0	0	0	56
8. Grass/bushes	–	0	0	0	4	0	0	16	4	16	0	0	40
9. Forest	–	0	0	0	0	16	0	0	28	4	4	0	52
10. Mixed land use	–	0	0	16	4	4	0	0	8	136	0	0	168
11. Kurnub K2	–	0	0	4	0	0	0	0	0	0	44	12	60
12. Kurnub K1	–	0	0	0	0	0	0	0	4	0	0	20	24
Sum	–	48	48	80	160	96	48	64	64	176	64	32	880

Colour aerial photographs (1:10,000)

For a section of the test site (about 50 km^2), colour aerial photographs (Camera Type: Wild 15/4 UAG-S, No 13280, focal length 153.28) with the scale 1:10,000 acquired in September 2000 were processed. The colour negatives were scanned with a photogrammetric precision scanner with a scanning resolution of 20 μm resulting in a ground pixel resolution of 0.20 m. A collection of the three karst levels was mapped as GPS points and compared with the texture they produce on the orthophotos, in order to provide a basis for developing a comprehensive interpretation key for the specific karst levels of the test site (Fig. 5). The karstified areas were delineated based on their specific texture and finally classified in general karst-level classes as described in the used vulnerability approach (PI-method) developed by Goldscheider et al. (2002). The results of the on-screen digitising of the karst levels (Fig. 6) were transferred to the whole test site; the dominating karst level of each individual formation was assumed to exist area-wide in that specific formation.

The thematic layer of the karstification was imported to ArcGIS and overlaid by geological information to compare the degree of karstification between the single aquifers. The results clearly indicate that, over the massive limestones (A7 aquifer), a general high degree of karstification (epikarst strongly developed, not sealed) exists. The Hummar formation (A4) is, in general, strongly karstified whereas the Na'ur Formation (A1/A2) is predominately moderately karstified. The orthophotos were used also for the location, size and shape of 'point' hazards (such as detached houses) within the hazard mapping procedure.

Table 2 Results of statistical calculations of the supervised classification of the LANDSAT ETM+ data

Overall accuracy: 69.5%	Producer accuracy (%)	User accuracy (%)
Water		
Urban (dense)	66.7	100
Urban	75	69.2
Agricultural areas	70	82.3
Limestone south	92.5	59.7
Limestone north	58.3	70.0
Quarry/bright limestone	83.3	71.4
Grass/bushes	25.0	40.0
Forest	43.8	53.8
Mixed land use	77.3	80.9
Kurnub K2	68.5	73.3
Kurnub K1	62.5	83.3
Kappa coefficient	0.65	

Additional spatial and non-spatial data

Several parameters used for the groundwater vulnerability assessment are based on information beneath the Earth's surface, namely the subsurface (e.g. unsaturated zone) and the underground (e.g. aquifer characteristics, thickness of geological units) that cannot be provided or replaced directly or indirectly by remote sensing data. Due to this fact, additional information from field investigations, GPS acquired field data, elevation information, topographic maps, hydrogeological and hydrological data and hazard characteristics had to be included. A high-resolution digital terrain model (DTM; 15 m) of the test site was generated within ArcGIS based on digitised topographic contour lines with an elevation interval of 20 m. A 1:50,000-scale soil map was drafted based on the Jordanian Soil Atlas (National Soil Map Project, Ministry of Agriculture 1994) and field investigations including soil thickness and soil characteristics were preformed. Soil samples were taken and infiltrometer tests and soil coring were accomplished at representative locations. The soil samples were analysed for standard parameters (pH, cation exchange capacity, particle size distribution, bulk density, pore

 DOI 10.1007/s10040-007-0202-0

Orthophotos	Interpretation key for the test site	Corresponding karst levels in the vulnerability method of Goldscheider (2002)
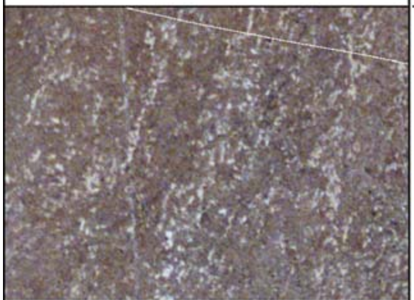 image section ~ 60 m	limestone partly covered by soil, surface texture is smoother due to little distinctive dissolution features like karren or widened fractures	moderately karstic or karst features mostly sealed
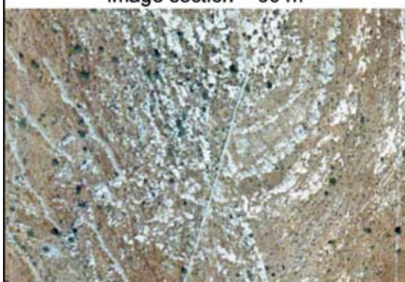 image section ~ 70 m	abrupt changes of tonal variations between the limestones and the dissolution features or fractures that are filled with soil producing a rougher surface texture, partly sparse soil cover	strongly fractured or strongly karstified and not sealed
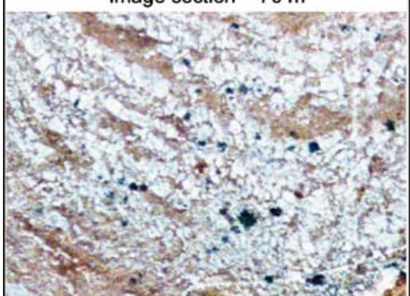 image section ~ 50 m	blocky appearance of the limestones due to intensive fracturing and karstification, partly very rough texture due to dense karst pattern, soil cover is often missing	epikarst, strongly developed, not sealed

Fig. 5 Developed interpretation key for the classification of the three levels of karstification and general karst level description in the vulnerability approach of Goldscheider et al. (2002)

volume, and natural water content). The measured effective field capacity (EFC) of the soils was used as one parameter for the assessment of the groundwater vulnerability.

Groundwater vulnerability

Approach and mapping procedure

For the assessment of the groundwater vulnerability, the PI-method, an intrinsic vulnerability approach reported by Goldscheider et al. (2000) was applied. The intrinsic vulnerability of groundwater to contaminants is independent of the nature of the contaminants and depends on the geological, hydrological and hydrogeological characteristics of an area (Daly et al. 2002). Common methods for vulnerability mapping are not based on a physically established methodology, but rather result from the combination of factors that are assumed to have an influence on contamination transport and attenuation (Zwahlen 2004, Daly et al. 2002, Gogu and Dassargue 2001, Goldscheider et al. 2000, Magiera 2000, Doerflinger and Zwahlen 1998, Hölting et al. 1995, Rosen 1994, Vrba and Zaporozec 1994, Aller et al. 1987, Foster 1987).

The PI-method originally developed for European karstic areas is based on two main factors: the P-factor and the I-factor. The P-factor describes the protective function of all layers existing between the water table and the Earth surface including the properties of the soil and the geological materials. Factors influencing the protective function of the overlying layers comprise: (1) the thickness and effective field capacity of the topsoil; (2) the recharge rate per year; (3) the thickness and grain size distribution of the subsoil; and (4) the lithology and degree of fracturing of the rocks. The protective function of the rock cover above the aquifer is determined by a point-counting system, whereas higher points of the specific factors express a higher protective cover function. The I-factor expresses the degree to which the protective cover is bypassed by lateral surface and subsurface. It also describes the infiltration conditions

 DOI 10.1007/s10040-007-0202-0

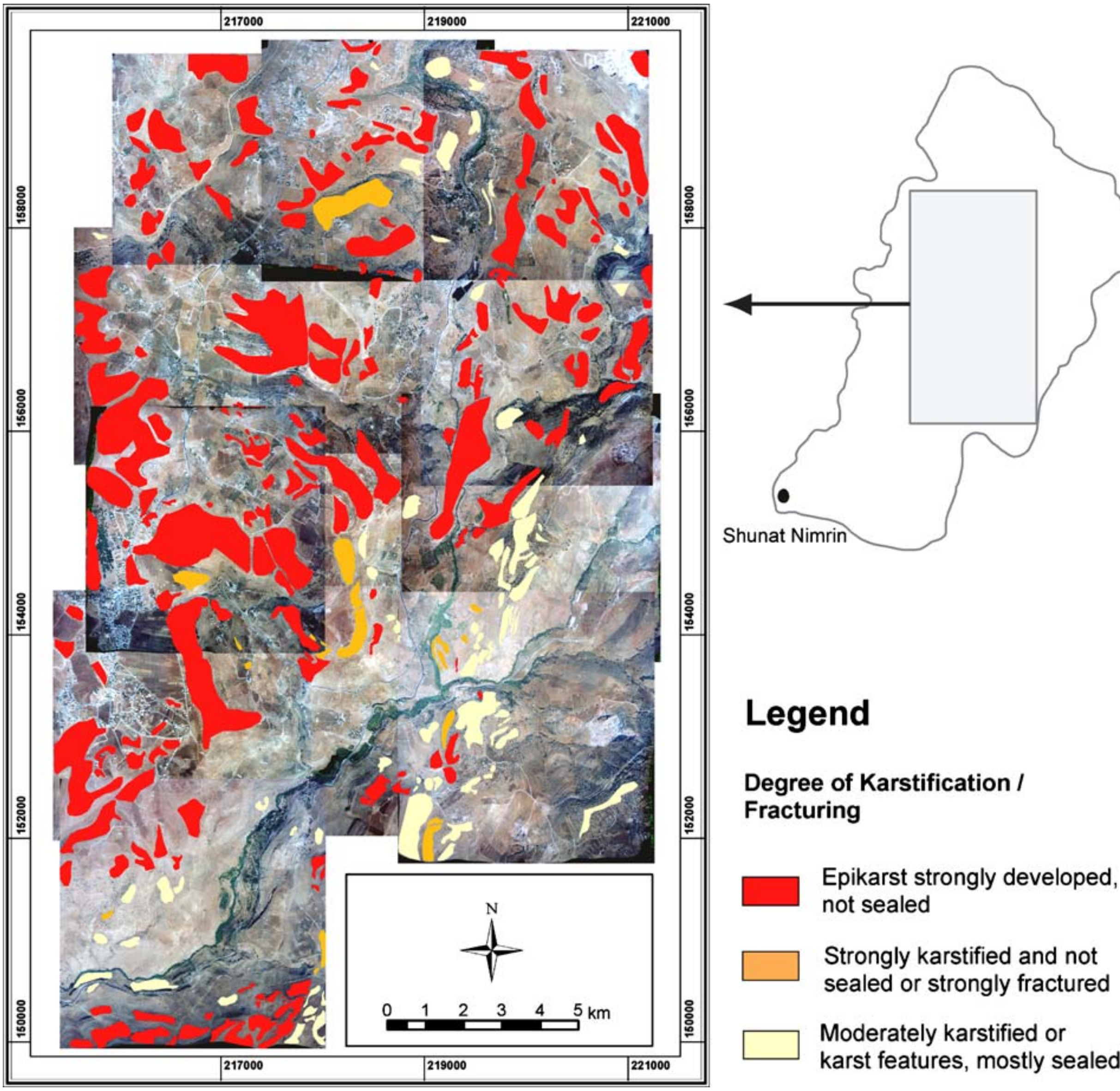

Fig. 6 Digital orthophotos (1:10,000) digitised thematic layer showing three levels of karstification, (indicated by *red*, *orange* and *yellow*). The index map in the upper right shows the section in the study area (*grey box*) for which digital colour orthophotos exist

showing the degree to which the protective cover is bypassed as a result of subsurface and lateral surface flow (Goldscheider et al. 2000). It takes into consideration the flow concentration of the surface water depending on the slope, soil properties and land cover conditions resulting in a factor with values between 0 and 1. The final vulnerability map is calculated by multiplying the points of thematic maps of the P-factor and the I-factor leading to the PI-factor that indicates the groundwater vulnerability. The higher the PI factor, the higher the protective function and hence the lower the vulnerability of the uppermost aquifer.

The groundwater vulnerability map was generated based on thematic layers derived from the processed remote sensing data, from soil investigations, from field survey data including existing hydrogeological and hydrological data, DTM data and geological maps. Due to the rapidly changing land cover conditions over short distances, the more detailed land use maps gained by on-screen digitising of the orthophotos were favoured over the LANDSAT ETM^+ data interpretation results. The agricultural layers were combined with the individual effective field capacities (EFC). For the recharge volume in the test site precipitation modeling results of Orthofer et al. (2001) were used, taking into account that only approximately 12% of the precipitation can be assumed for groundwater recharge (Ta'any 1992). Very limited and small subsoil deposits (wadi floor deposits) exist beneath the Wadi Shu'ayb course (Al-Daher, University of Amman, Jordan unpublished data, 1989); since they are of no significance for the protective function of the groundwater they are not considered as a special layer. The lithology was taken from existing geological maps and studies (Ta'any 1992). The degree of karstifica-

 DOI 10.1007/s10040-007-0202-0

tion was assessed based on the high-resolution orthophotos analysis.

The thickness of the unsaturated zone of the karstified aquifers was assessed based on well data (open files, kindly provided by the Ammam Ministry of Water and Irrigation (MWI), personal communication, 2002) and the topography and elevation of the discharging springs. For the I- factor (infiltration conditions), the saturated infiltration rates of the soils were taken based on the granulometric curves of soil samples taken in the test site (Table 3).

The depth to the low-permeability layers was determined based on the soil map and soil coring results. To assess the overland flow over paved surfaces (frequently Hortonian), the urban areas classified on the supervised LANDSAT ETM$^+$ were combined with the soil map. The I-factor distinguishes between two types of vegetation cover: forest and field/meadow/pasture. Under moderate European climate conditions, woodlands infiltration is enhanced because of the characteristics of the forest soil (loose organic material, abundant macro pores) and due to the reduction of the precipitation intensity through interception. Agricultural areas often enhance surface runoff due to the soil characteristics (clayey, loamy soils) and increased compaction of the not permanently vegetated surface. In Jordan, no woodland comparable to a typical European forest exists. Oak and pine tree forests grow directly on more or less karstified limestone and hardly any soil cover is present. Therefore, the forest areas were not assigned lower values due to the higher infiltration capacity as normally intended by the PI-method. The forest is, instead, treated as equal with the field/grassland/pasture areas.

No swallow holes or sinking streams exist in the test site, but deep wadis can be considered as potentially more vulnerable zones, since they are often deeply incised into the aquifer and the depth to the water table is less. Many wadis follow the direction of faults and indicate higher permeable zones. Further investigations have to be done to assess whether zones under the wadi beds are more permeable and possibly lead to direct and fast infiltration of contaminated water into the aquifer.

Table 3 Saturated infiltration rates (after DIN 4022, Deutsches Institut für Normung e.V. [Federal German Institute for Engineering Standards] 1987) in the test site for different soil locations (modified after Kuntz, University of Karlsruhe, unpublished data, 2003)

Location	Saturated infiltration rates	
	(mm/hr)	(m/s)
PL–1	199	2.8×10^{-6}
PL-2	252	7.0×10^{-5}
PL-3 N	180	5.0×10^{-5}
PL-4	180	5.0×10^{-5}
PL-5	12	3.3×10^{-6}
PL-6	119	3.3×10^{-5}
PL-9 (& PL-7)	241	6.7×10^{-5}
SL-1	47	1.3×10^{-5}
SL-3	202	5.6×10^{-5}

A map of soil test locations is given as Electronic supplementary material.

The groundwater vulnerability map

The P-map shows a dominating moderate and a very low protective function of the protective layers that matches with the outcrops of mainly bare karstified limestones and dolomites with well-developed karst features and only patchy or missing soil cover (Fig. 7a). Due to different hydrogeologic characteristics, a high protective function exists where the Kurnub sandstone crops out. In general, the contribution of the topsoil to the protective function of the aquifers is very small. A total of 82.9% of the area has no assigned protection points for the topsoil layer due to the absence of a continuous soil cover. The class "very high protective function" does not exist at all in the test site.

The I-map includes the range of infiltration or bypass probabilities, from very low to high. The very low and a low degree dominate. Areas with a very low degree of bypassing mainly exist over bare karst where the main flow process is infiltration. The few areas with a very high degree of bypassing are limited to steep slopes favouring surface flow and to missing soil cover leading to a fast surface or subsurface flow.

After the P-map and the I-map are combined to form the vulnerability map, the effect of the infiltration conditions is visible mainly in areas that show a moderate protective function in the P-map, and is reduced by a high degree of bypassing (low I-factor). Thus they are assigned to highly vulnerable areas. In general the influence of the I-factor is low (Fig. 7b). About one third of the area shows a high vulnerability due to different reasons: a large portion of outcrops of bare or patchy covered highly karstified rocks, a missing continuous soil cover, steep slopes that favour a bypassing of the protective functions (Fig. 7c). Areas with "very low vulnerability" do not exist at all.

Groundwater hazards

Approach and mapping procedure

The hazards in the test site were evaluated using the guidelines of the COST Action 620 (De Katelaere et al. 2004). Figure 8 shows a schematic illustration of the expected hazard types in the test site. According to their geometrical features, hazards can be differentiated in punctiform (e.g. septic tanks), linear (e.g. streets) and polygonal hazards (e.g. agricultural area). They are strongly dependent on the mapping scale.

In the hazard inventory list of the COST Action 620, hazards are first divided into three main categories (level I), which are based on the type of land use: agricultural activities, infrastructure development (detailed in Fig. 9), and industrial activities. The main categories are further divided in subcategories (level II), making use of additional criteria. The subcategories distinguish between hazards according to the main source of possible groundwater contamination (solid or liquid contaminants), or refer to types of industrial or agricultural activities and their corresponding spectrum of possible pollutants. A

 DOI 10.1007/s10040-007-0202-0

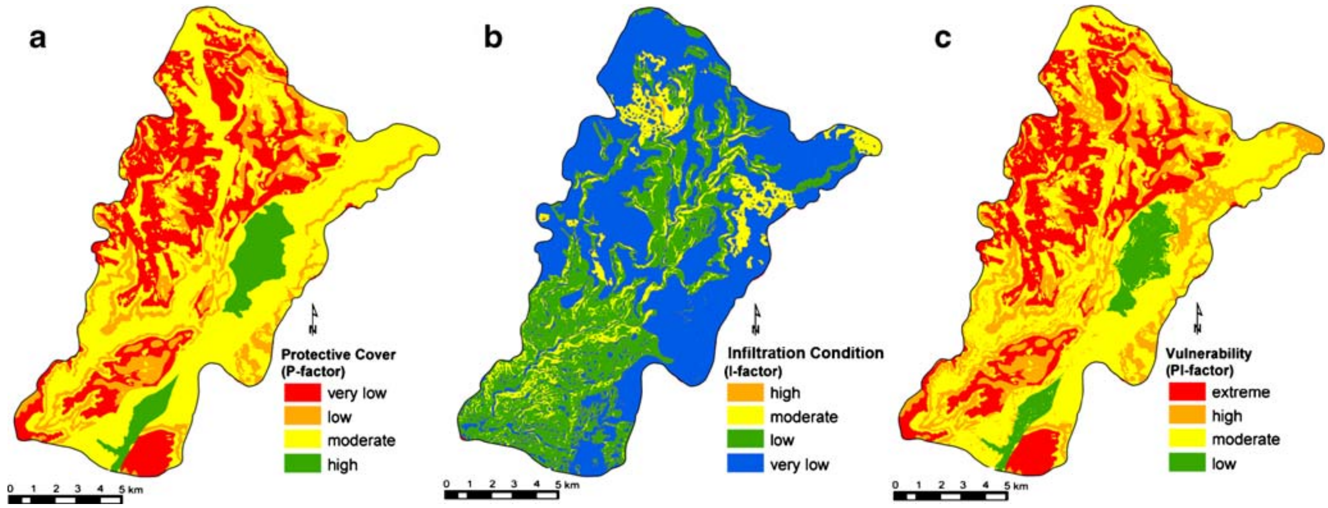

Fig. 7 **a** P-factor map showing the protective cover effectivity, **b** I-map showing the infiltration conditions expressed as degree of bypassing and **c** vulnerability (PI) map of the test site

further subdivision of the subcategories is made indicating all possible existing types of hazards within each subcategory (level III). This leads to the weighting value of each hazard.

In the first step, an unclassified hazard map is constructed displaying the existing hazard types, their location and size via the use of special graphic symbols or signatures delineated by De Ketelaere et al. (2004) in a hazard inventory list. In the second step, a classified hazard map is generated showing the degree of harmfulness of the hazards for the groundwater expressed as a hazard index (HI). The HI is determined in a weighting, ranking and reduction scheme.

The weighting factor is a relative, non-measurable value between 0 and 100 defined in the COST Action 620 hazard inventory list. This list includes about 100 possible hazards. Since it is nearly impossible to establish quantitative methods to arrive at an absolute measure of the degree of harmfulness of a substance, the main criteria for the weighting value concerns the toxicity of relevant substances associated with each type of hazard, as well as their properties regarding solubility and mobility. Besides that, the weighting values of the hazards consider special and dangerous substances, organic and non-organic wastewater and large surface contamination calculated with a formula based on the SINTACS vulnerability scheme (Civita and De Maio 2000). This scheme is based on the EU Directive on toxic sources of contamination (De Ketelaere et al. 2004). A "contamination index" is calculated for each hazard by adding up the potential "environmental impacts caused by specific human activities". A low weighting factor is assigned to hazards with a low degree of harmfulness, e.g. greenhouses (weighting factor=20). High weighting values are assigned to hazards

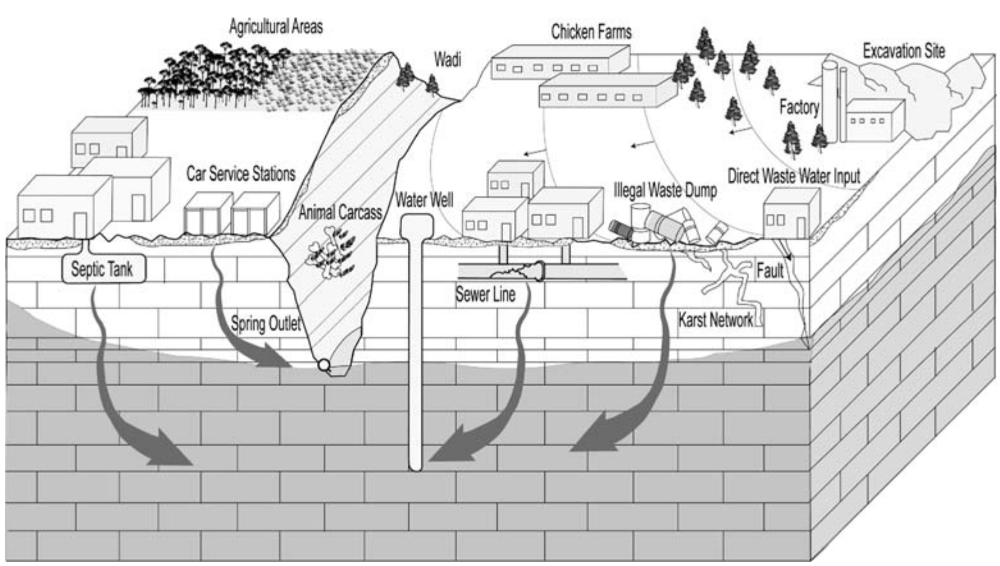

Fig. 8 Schematic illustration of the main hazards that exist in the test site

 DOI 10.1007/s10040-007-0202-0

Number	Level I. Categories of hazards	Level II. Subcategories of hazards	Level III. Hazard Type (Number 1.2)	Weighting value of each Level III hazard
1	*Infrastructural development*		…	
1.1		Waste water	Garbage dump	40
1.2		Municipal waste	Waste loading station	40
1.3		Fuels	Sanitary landfill	50
1.4		Transport / traffic	Spoils depository	35
1.5		Recreational facilities	Sludge from treatment plants	35
1.6		Diverse hazards	…	

Fig. 9 First (I) and second (II) level of hazard classification for Infrastructural Development. Level II hazard type municipal waste and its level III subcategories (*grey shaded*) are shown as examples (modified after De Katelaere et al 2004)

that have a high degree of harmfulness, e.g. oil refinery, or a wastewater injection well (weighting factor=85).

After the weighting factor is determined, it is multiplied with a ranking factor (Q_N) between 0.8 and 1.2, to cope with the differences between various hazard types of the same group. Thus, the weighting factor can be raised or reduced by the ranking factor. Finally, a reduction factor (R_f) in the range of 0 and 1 is included to consider status, maintenance, age, security measures, etc., that exist at a location, including the probability that a hazard release might take place. If there is no information available about devices or measures that are known to reduce the likelihood of an impact to the groundwater, the reduction factor is set to 1. Consequently, the final hazard index (HI) is calculated using the following formula:

$$HI = H \cdot Q_N \cdot R_f, \quad (1)$$

Where H is the weighting factor, Q_N is the ranking factor, R_f is the reduction factor.

The location, size and extent of the hazards were determined by fieldwork using GPS and the thematic layers gained by the remote sensing analysis. The LANDSAT EMT^+ data comprised polygons representing the location and extent of big hazards such as cement factories, excavation sites and urban areas. The black and white orthophotos were used for mapping animal barns, chicken farms, crops and orchard areas, wastewater treatment plants and road networks. The higher resolution colour orthophotos were used to locate and map detached houses. After generating the unclassified hazard map showing size, position and type of hazard as a symbol, the classified hazard map was generated classifying each hazard type with the predefined hazard index HI (Fig. 10a). Table 4 lists the mapped hazard types, their weighting value (H) and ranking (R_N) and the number of individual hazard types.

The COST Action 620 guidelines were modified for the HI calculation in urban areas. According to the guidelines, two different weighting values that represent a wide span are available for urban areas: areas with leaking sewer pipes and sewer systems (H=35), and areas without sewer systems (H=70). Only the average percentage values of the municipalities regarding houses with connection to the sewer system were available in the test site. Therefore, the HI was adjusted to the ratio of connected houses without including an additional ranking or reduction factor (Table 5).

Because a reduction factor could not be determined at all in the test site (except in two cases), due to missing information about hazard protective devices or measures, the reduction factor is not listed in Table 4. For a car service station equipped with a safety gully for the wastewater and a filling station equipped with a safety channel for wastewater, a reduction factor of 0.9 was allocated. For all other hazards, the reduction factor was set to 1.

The groundwater hazard map

In the test site 27 different hazard types were evaluated. The most prevalent types are small industries, agricultural and municipal hazards, and point-source contamination incidents that are, for example, caused by manure heaps and filling stations or oil pumps: industrial hazards form the majority (53%), followed by the agricultural hazards (28%) and the municipal hazards (19%). As some of the mapped hazards were not included in the inventory list of the COST Action 620 that was initially developed for European standards, the list had to be expanded to include, for example, car service and car washing stations and a locksmith. The unclassified map shows big differences in the development and degree of urbanisation and can be subdivided into (1) a highly urbanised northern part with a well-developed infrastructure, a settlement of certain industrial plants and a variety of agricultural activities and (2) an almost deserted southern part with no infrastructural facilities (Fig. 10). Accordingly, the hazards are concentrated in the larger villages in the northern part and around smaller villages in the centre of the study area. In general, the agricultural areas are affected only by a small or no degree of harmfulness. The prevalent industrial companies are rather small firms and garages. With respect to potential groundwater contamination, these facilities are problematic because of their unpaved floors, which contaminants (e.g. waste oil) can infiltrate.

 DOI 10.1007/s10040-007-0202-0

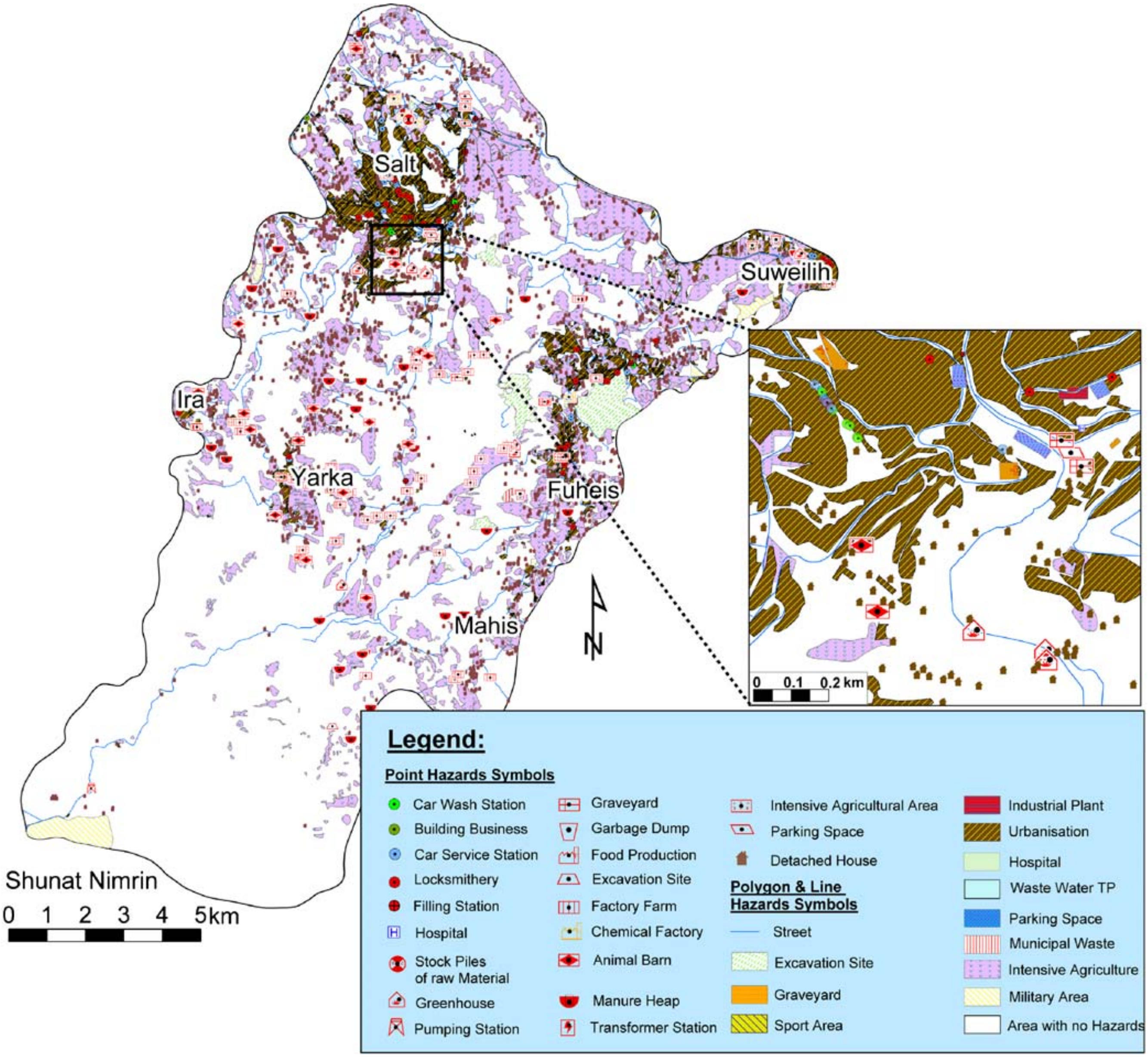

Fig. 10 Unclassified hazard map of the test site. The legend shows the point, line and polygonal hazard symbols of the unclassified hazards. A section of the map is shown at larger scale for the city of Salt. The hazards were originally mapped on the scale of 1:50,000; due to the reduction of the original scale some details are no longer recognisable in this illustration

For the classified hazard map, the vector map of unclassified hazards was converted into raster data with a chosen cell size of 25×25 m (edge length of 0.5 mm). The limit of the visibility of a single raster cell representing a point hazard in a 1:50,000 map is 225 m^2. The HI values are divided into five classes (1–5), ranging from "no or very low" to "very high" hazard level (with corresponding colours, shown in Fig. 12a). The highest hazard indices exist in the urban areas and arise from the calculation and sum of two or more hazard types within one raster cell. An example of a very high hazard index in the test site is the existence of a filling station with an unpaved floor in an urbanised area. In the case of coexistence of two or more hazards, hazard types which can coexist (e.g. fuel stations in an urban area) were added or ranked up, and hazard types which exclude each other (e.g. a factory farm over an intensive agriculture area) were assigned the highest of the possible weighting factors. Due to resolution and scale, very high HI areas barely appear on maps with scales bigger than 1:50,000, since very high HI areas are mostly point hazards; therefore, they are hardly visible on the map in Fig. 10a.

The Jordanian data policy cannot be compared to the situation in Europe, particularly Germany, where within given time periods, name and addresses of all firms as well as the type and amount of substances hazardous to groundwater are recorded and updated and a trade supervisory office provides databases with all office

Table 4 Hazard types, weighting value (*H*), ranking factor (Q_N), final calculated hazard index (HI) and number of occurrences of the hazard types; NN indicates that there are no hazards existing

Hazard type	H	Q_N	HI	No.	Hazard type	H	R_N	HI	No.
Animal barn	30	0.8	24	2	Intensive agricultural area	30	0.8	24	20
		0.9	27	14			1.0	30	35
		1.0	30	4					
Building business	40	1.0	40	2	Locksmith	35	0.9	32	28
		1.1	44	2			1.0	35	16
							1.1	39	2
							1.2	42	4
Car service station	45	0.8	36	8	Manure heap	45	0.8	36	14
		0.9	41	59			1.0	45	14
		1.0	45	10					
		1.1	50	9					
		1.2	54	13					
Car wash	40	0.9	36	8	Military area	35	1	35	7
		1.0	40	4			1.1	39	
		1.2	48	2					
Chemical factory	65	1.0	65	4	Garbage dump	40	0.8	32	1
		1.2	78	1			1.0	40	6
							1.2	48	2
Detached houses	45	–	45	NN	Parking space	35	1.0	35	4
							1.1	39	1
							1.2	42	1
Excavation site	25	0.8	20	3	Pumping station	65	1.0	65	1
		0.9	23	1					
		1.0	25	1					
		1.2	30	1					
Factory farm	30	1.0	30	20	Sport area	25	0.8	20	2
		1.1	33	35					
Filling station	60	1	60	9	Stock pile of raw material	60	1.2	72	1
		1.1	66	1					
		1.2	72	1					
Food production	45	1.0	45	1	Streets	40	0.9	32	NN
		1.1	50	1			1.0	40	
							1.1	48	
Graveyard	25	0.8	20	2	Transformer station	30	0.8	24	1
		0.9	23	7					
		1.0	25	4					
		1.1	28	14					
Greenhouse	20	1.0	20	11	Urban area with/without sewer system	35	[a]		NN
Hospital	35	1.0	35	2	Wastewater treatment plant	35	1	35	2
		1.2	42				1.0	39	1

[a] Special weighting and ranking procedure, see text for explanations

master data. In Jordan, environmental agencies that provide land registries, including all known contaminated sites or abandoned hazardous sites, do not exist. The fact that lists of the number, type, location, and size of industrial firms do not exist or were not available from public offices or ministries, and data about the state and age of plants are missing, can be considered as normal in areas comparable with the test site.

Table 5 Evaluated hazard index of urbanisation related to the percent of connected houses (in %) in the urban areas

Location	Connected houses (in %)	Hazard index (HI)
Mahis	90–100	35
Fuheis	90	38
Suweilih	60	49
Salt	50	53
Rural housing	0	70

Risk intensity

Approach and mapping procedure

The first step in risk assessment is identifying existing potential hazards and exposing pathways of groundwater contamination taking into account the likelihood of an impact, the intensity of a potential impact and the vulnerability of the groundwater. The risk intensity map, a result of the combination of the groundwater vulnerability and hazard maps, shows the interaction between the surface contamination load and the aquifer pollution vulnerability at the location concerned. Thus, the risk intensity map reflects the probability of groundwater to be actually contaminated by human activities. This shows that the highest risk of contamination exists when a dangerous hazard is located in zones which are characterised by highly vulnerable aquifers. Guidelines for the assessment of the risk intensity are given by Hötzl et al. (2004) for the COST Action 620 (Zwahlen 2004).

 DOI 10.1007/s10040-007-0202-0

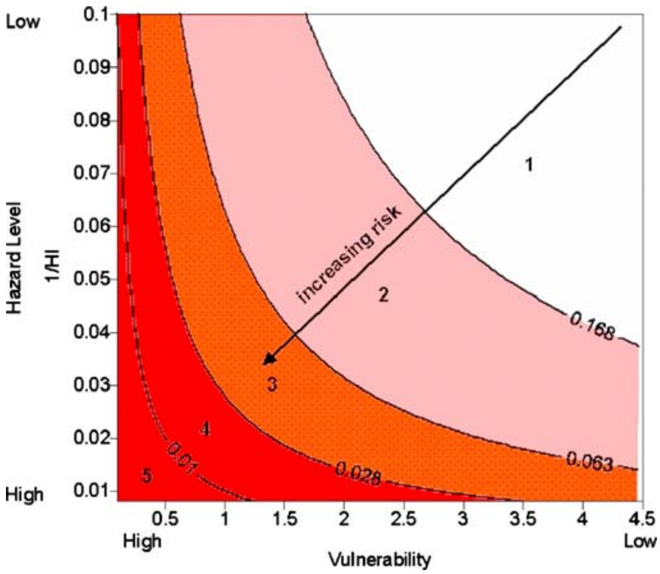

Fig. 11 Diagram of risk intensity index calculated by equation (2). Five classes were assigned to build risk levels (after Hötzl et al. 2004). Increasing risk within the classes is shown in the diagram by *gradually darker red tones*. Higher numerical vulnerability values indicate a lower risk that the aquifer will be contaminated, but higher numerical hazard index values represent a higher probability that a possible hazard can be released

The risk intensity map is based on the risk intensity index (RII), which is unitless and calculated by multiplying the reciprocal value of the hazard indices (HI) with the PI-factor (π) of the groundwater vulnerability map using the formula indicated by Hötzl et al (2004):

$$RII = \frac{1}{HI} \times \pi \quad (2)$$

The reciprocal hazard index is used since the hazard index and the PI-factor of the groundwater vulnerability map tend towards the opposite direction with higher risk (Fig. 12). Higher numerical vulnerability values indicate a lower risk that the aquifer will be contaminated, but higher numerical hazard index values represent a higher probability that a possible hazard can be released.

The risk intensity map

Unlike the groundwater vulnerability map that is quasi timelessly valid due to the fixed natural hydrogeological and hydrological setting, due to modification in the hazards that can be potentially released, the risk intensity map can change if the classified hazard map changes. The highest risk intensity exists in urban areas where concentrations of different hazard types assigned to a high hazard index are located over karstified limestone with low protective cover (Fig. 10b). In places where the hazard map shows no or only slight variations of the hazard index (e.g. agricultural areas), the variations in the risk intensity level are caused by different vulnerability classes.

Even though there are few industrial activities and a very low-hazard level prevails in the test site, there are some "hot spots" of contamination that produce, combined with a high groundwater vulnerability, a very high-risk intensity for the groundwater. The hazard map in combination with the groundwater vulnerability map is an important tool to carry out a risk intensity assessment that increases the awareness of the public to reduce existing hazards and to avoid further contamination of the groundwater.

Discussion

Transferability and applicability of the European approaches

The application and transferability of the European vulnerability approach in a test site in the Middle East proved in general to be good and satisfying, with some minor constraints that should be considered. The as-

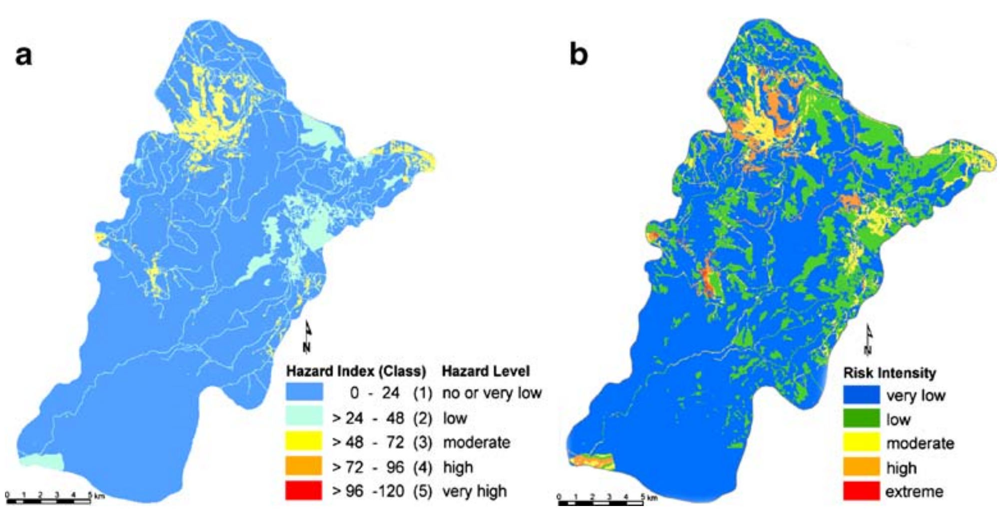

Fig. 12 **a** Classified hazard map and **b** risk intensity map of the test site

DOI 10.1007/s10040-007-0202-0

sumption that forest cover favours infiltration, whereas agricultural areas are more likely to produce surface runoff (Goldscheider et al. 2000), cannot be applied in the test site, due to the different characteristics of the forest and soil in (semi) arid areas like Jordan. The recharge range of the PI-method does not mirror the climatic situation of (semi) arid Mediterranean climate zones and thus does not differentiate recharge amounts below 100 mm/a. The recharge range has to be expanded to include smaller amounts with finer grading to mirror the situation more accurately. In the test site, on steep valley slopes, terracing practices for orchards are commonly used to reduce surface runoff and soil erosion. In the PI method, steep slopes are given low ratings. This assumption is based on the fact that surface contaminants deposited on sites having steep slopes will tend to runoff rather than stand long enough to infiltrate (Aller et al. 1987). Terracing, of course, dramatically alters slope, converting a formerly steep slope to a nearly flat area. Most topographic maps and accordingly DTMs based on these maps, rarely depict terracing (Merchant 1994). The rating of the slope angle ought to be adjusted upwards to account for terracing. However, the points discussed above do not adulterate the qualitative results of the PI-method, but rather shift the results slightly to higher or lower total points. The score of the classes of the PI-method include a relatively wide span; each class of the P-factor covers a score range of one magnitude (Goldscheider et al. 2000). Therefore, the shifted score results are normally buffered and do not lead to an upgrade or downgrade to the next vulnerability class.

The hazard inventory list of the COST Action 620 was developed from scientists of several European countries and therefore does not take into account any country-specific characteristics. Consequently, the hazard mapping instructions are relatively general and unspecific. The elaboration represents the current situation of potential hazards, whereas the type of hazards or the corresponding degree of harmfulness may partly change in the future due to infrastructural or industrial development. The hazard-ranking factor is difficult to define and it is difficult to give meaningful reasons for the chosen value between the 0.8 and 1.2. Often the use of the ranking factor proved to have no influence on the final hazard index value. The hazard approach does not encompass every existing hazard type because the hazard map should be clear and easy to understand, and “over-classification” in too many hazard classes is not allowed. Therefore additional hazard types that exist in the test site have to be adapted to the COST Action 620 list. In industrial zones or dense urban areas with a high density of hazards, the overlap between different hazard type symbols reduces the ability to recognise the individual hazard symbols and limits the use of the unclassified hazard map. In this case, it would be better to classify the whole industrial area as a polygonal hazard and display only special hazards with a significant hazard index such as fuel stations, with an individual point symbol.

From a groundwater protection and groundwater management point of view, it is very important to have precise information about where potential hazards are located and where hazardous events may occur. The COST Action 620 offers a relatively simple method to assign the existing individual hazards to the associated hazard type of the inventory list. Due to the limited number of hazard types, the resulting unclassified hazard map is quite simple and easy to read and understand. The simplicity of the hazard map is indispensable if the map is to serve as an efficient tool in planning and decision-making processes for planners, consultants and stakeholders for both national and local entities as an integral component of environmental impact studies (De Ketelaere et al. 2004).

Usefulness of remote sensing data and choice of the data type

The LANDSAT ETM$^+$ image gave a good up-to-date overview of the land cover and land use situation and infiltration conditions in the test site and was used to map big polygonal hazards such as urban areas or quarries. The speed at which the digital image processing of the LANDSAT ETM$^+$ could produce thematic maps by automatic classification, was much faster than the analysis of the panchromatic orthophotos by on-screen digitisation. One main advantage of the LANDSAT satellite data is the worldwide availability of most recent ETM$^+$ imagery, whereas aerial photographs are often limited in actuality and coverage or in some countries are not made available for political or security reasons. Scale restricts type, quantity, and quality of data (Star and Estes 1990), thus the appropriate map scale must fit the level of detail required in the project. Different data types have to be considered dependant on the desired scale for the risk intensity map, giving either a general overview or providing site-specific information. The use of LANDSAT ETM$^+$ data is suitable for map scales equal to or smaller than 1:50,000. Aerial photographs are dependant on their resolution and are also suitable for larger map scales, e.g. 1:25,000, 1:10,000 or even larger.

Concerning the relatively small size of the test site, with a high spatial heterogeneity, aerial photographs have one major advantage over the LANDSAT ETM$^+$ data: a higher spatial resolution (an order of magnitude better, less than 1 m versus 15/30 m) that allows a more detailed interpretation of small features like karst forms, small and individual agricultural areas, woodlands, streets and the detection of detached houses. In the case of bigger areas of interest (larger than 5,000 km^2) with homogenous land cover such as the flat areas in the Jordan Rift Valley and desired mapping results of 1:100,000 including detailed maps of critical areas, a hierarchical approach is recommended. The hierarchical approach investigates phenomena at an intermediate scale and information regarding potential critical areas is used for further investigations at a lower scale with high or very high spatial resolution data that could be used for 1:10,000 detail maps. High-resolution satellite data can be provided nowadays, for example by the IKONOS and Quick Bird satellite sensors, which guarantee highly accurate, commercial multispectral imagery. For very detailed maps of 1:5,000 up to 1:1,000, high quality digital aerial photographs with corresponding scales should be favoured.

For groundwater vulnerability mapping, remote sensing data play mainly the role of allocation or supplementation of missing topographic maps or general land cover and land use information, and also (if possible) of lithological or surface structural features (fracturing, faults, and karstification) that can be used to asses the infiltration conditions. In the case of hazard assessment, remote sensing data proved to be very useful for the unclassified hazard map, indicating location, size, and extent of many hazards like agricultural areas, excavation sites, street networks, urban areas, wastewater treatment plants, animal barns and detached houses. The detection of hazard types by remote sensing is only possible if the hazards exhibit distinct characteristics that can be recognised on the images by their spectral characteristics, tone, texture, pattern, shape and size or other associated characteristics. Several parameters that are important for vulnerability are based on information beneath the Earth's surface namely, the subsurface (e.g. unsaturated zone) and the underground (e.g. aquifer characteristics, thickness of geological units) that cannot be provided or replaced directly by remote sensing data due to the fact that passive sensors have no ground penetrating capabilities. Some parameters solely can be obtained by other field or laboratory measurements. Sometimes, second-order or indirect indicators on remote sensing images allow a qualitative assessment of the hydrogeological characteristics of an area such as regional structural features, weathering and karstification, vegetation, drainage density, sinkholes or faults. In summary, remote sensing data cannot be used as a stand-alone technique able to replace completely conventional data acquisition needed for groundwater-risk intensity mapping, but the combination of remotely sensed data with ancillary data has shown a high potential to provide reasonably accurate information and to enhance and supplement thematic information for groundwater risk intensity.

Summary and conclusions

The combination of remote sensing data, GPS information, field investigations and collateral data for an integrated use in a GIS proved to be an efficient tool for the generation of risk-intensity maps. In the test site, karstified Upper Cretaceous limestone with missing soil cover is extremely or highly vulnerable to contamination because the protective function of the layers is very low. The dominating hazards in the test site are small industries, agricultural and municipal hazards, and point-source contamination that is caused, for example, by manure heaps, filling stations, septic tanks or oil pumps. Low risk intensity areas are dominated by agricultural areas since there is not much use of agro-chemicals and because of the moderate-to-thick soil cover that is present. In the urban areas and their surroundings, moderate to high-risk intensity is present, since concentrations of different hazard types, assigned to a high hazard index, are located over karstified limestone showing a high vulnerability. In urban areas especially, there is an urgent need for a more integrated approach to the management of groundwater and wastewater interactions and for the cooperation between public and private systems. Thus, the mapping results can help decision makers to understand the interactions between surface water, groundwater, and the environmental system.

There is a call for action on illegal waste dumps, connection of more households to the sewer system, and wastewater treatment plants (or to convert septic tanks to cesspits, designed as sealed disposal units). Direct waste deposition and wastewater injection into the karst fractures or widened joints of the limestones, or the disposal of animal carcasses in wadi beds or karst formations should be prevented. With the results of tracer tests, groundwater protection areas should be established that can help to reduce microbiological contamination.

An updated inventory of all hazardous sites and an assessment of the hazards posed from existing human activities are necessary for all national environmental objectives for surface water, groundwater and ecosystems and groundwater protection schemes. The risk intensity map indicates problematic areas where effort should be made to reduce existing hazards and to prevent or minimise the probability of a contamination event and its consequences by implementing special actions. The risk-intensity map can also be used to increase the awareness of the Jordanian people on how their activities can pose a threat to groundwater. The delineation of country-wide groundwater risk intensity maps can be the first step to assess the status and risk of groundwater and consequently the results can be used as a basis for groundwater management strategies.

Acknowledgements The study was done within the framework of the multi-lateral project: Water Resources Evaluation for a Sustainable Development in the Jordan Rift Basin, German-Jordanian-Israeli-Palestinian Joint Research Program funded and supported by the German Ministry of Education and Research (BMBF 02WT0160) and the Israeli Ministry of Science (MOS). The authors would like to thank the BMBF, the MOS, and all project partners for the helpful discussions and their support during the years of scientific cooperation and friendship. The authors also wish to express their thanks to Prof. Elias Salameh of the University in Amman (Jordan) for his support throughout the field surveys and the research in Amman.

References

Al-Adamat RAN, Foster IDL, Baban SMJ (2003) Groundwater vulnerability and risk mapping for the Basaltic aquifer of the Azraq basin of Jordan using GIS, remote sensing and DRASTIC. Appl Geogr 23(4):303–324

Al-Farajat M (2001) Hydrogeo-eco-systems in Aqaba/Jordan coasts and region: natural settings, impacts of land use, spatial

 DOI 10.1007/s10040-007-0202-0

vulnerability to pollution and sustainable management. Forschsergeb Bereich Hydrogeol Umwelt 30:220
Al-Kharabsheh-Atef A (1999) Influence of long-term overpumping on groundwater quality at Dhuleil Basin, Jordan. Forschsergeb Bereich Hydrogeol Umwelt 18:2.1–2.10
Aller L, Bennet T, Lehr JH, Petty RJ (1987) DRASTIC: a standardised system for evaluating groundwater pollution potential using hydrologic settings. EPA/600/2-85/0108, USEPA, Robert S. Kerr Environmental Research Laboratory, Ada, OK, 163 pp
Basnyat P, Teeter LD, Lockaby BG, Flynn KM (2000) The use of remote sensing and GIS in watershed level analyses of non-point source pollution problems. For Ecol Manage 128(1):65–73
Bender F (1974) Geology of Jordan. Borntraeger, Berlin, 196 pp
Bressan MA, Dos Anjos CE (2003) Techniques of remote sensing applied to the environmental analysis of part of an aquifer located in the Sao Jose dos Campos Region sp, Brazil. Environ Monit Assess 84(1–2):99–109
Bukata RP, Jerome JH, Kondratyev KY, Pozdnyakov DV (1991) Estimation of organic and inorganic matter in inland waters: optical cross sections of Lakes Ontario and Ladoga. J Great Lakes Res 17:461–469
Chebaane M, El-Naser H, Fitch J, Hijazi A, Jabbarin A (2004) Participatory groundwater management in Jordan: development and analysis of options. Hydrogeol J 12(1):14–32
Chowdary VM, Yatindranath Kar S, Adiga S (2004) Modeling of non-point source pollution in a watershed using remote sensing and GIS. Photonirvachak 32(1):59–73
Civita M, De Maio M (2000) Valutazione e cartografia automatica della vulnerabilità degli acquiferi all'inquinamento con il systema parametrico SINTACS R5. Bologna (Pitagora Editrice), 248 pp
Davenport IJ, Silgram M, Robinson JS, Lamb A, Settle JJ, Willig A (2003) The use of earth observation techniques to improve catchment-scale pollution predictions. Phys Chem Earth 28:1365–1376
Daly D, Dassargues A, Drew D, Dunne S, Goldscheider N, Neale S, Popescu IC, Zwahlen F (2002) Main concepts of the European approach for (karst) groundwater vulnerability assessment and mapping. Hydrogeol J 10(2):340–345
Dekker AG, Malthus TJ, Hoogenboom HJ (1995) The remote sensing of inland water quality. In: Danson FM, Plummer SE (eds) Advances in remote sensing. Wiley, Chichester, pp 123–142
De Ketelaere D, Hötzl H, Neukum C, Civita M, Sappa G (2004) Hazard Analysis and Mapping. In: Zwahlen F (ed) COST Action 620: vulnerability and risk mapping for the protection of carbonate (karst) aquifers. Final Report, Office of the Official Publications of the European Communities, Brussels, Belgium, 297 pp
Deutsches Institut für Normung e.V. (1987) DIN 4022, Baugrund und Grundwasser, Benennen und Beschreiben von Boden und Fels, Beuth, Berlin, 28 pp
Doerflinger N, Zwahlen F (1998) Practical guide: groundwater vulnerability mapping in karstic regions (EPIK). Swiss Agency for the Environment, Forests and Landscape (SAEFL), Bern, Switzerland, 56 pp
Dottridge J, Jaber-Abu-Nizar (1999) Groundwater resources and quality in northeastern Jordan: safe yield and sustainability. Appl Geogr 19(4):313–323
D'Sa EJ, Zaitzeff JB, Steward RG (2000) Monitoring water quality in Florida Bay with remotely sensed salinity and in situ bio-optical observations. Int J Remote Sens 21(4):811–816
Ellyett CD, Pratt DA (1975) A Review of the potential applications of remote sensing techniques to hydrogeological studies in Australia. Technical Paper No. 13, Australian Water Resources Council, Australian Governmental Publishing Service, Canberra, 147 pp
Engman ET, Gurney RJ (1991) Remote sensing in hydrology. Chapman and Hall, London, 250 pp
Foster SSD (1987) Fundamental concepts in aquifer vulnerability, pollution risk and protection strategy. Vulnerability of soil and groundwater to pollutants ed. Proceedings and information committee for hydrological research, TNO committee on Hydrological Research, The Hague, pp 69–86
Farrell SO (1985) Evaluation of color infrared aerial surveys of wastewater soil absorption systems. EPA/600/2-85/039 (NTIS PB85-189074), USEPA, Washington, DC, 40 pp
Finkbeiner M, O'Tool MM (1985) Application of aerial photography in assessing environmental hazards and monitoring cleanup operations at hazardous waste sites. Paper presented at The 6th National Conference on Management of Uncontrolled Hazardous Waste Site. USEPA, Silver Spring, MD, November 1985
Gogu R, Dassargues A, (2001) Intrinsic vulnerability maps of a karstic aquifer as obtained by five different assessment techniques: comparison and comments. Proc. of the 7th Conference on Limestone Hydrology and Fissured Media, September 2001, Besançon, France, pp 161–166
Goldscheider N (2002) Hydrogeology and vulnerability of karst systems: examples from the Northern Alps and the Swabian Alb. PhD Thesis, University of Karlsruhe, Germany
Goldscheider N, Klute M, Sturm S, Hötzl H (2000) The PI method: a GIS based approach to mapping groundwater vulnerability with special considerations of karst aquifers. Z Angew Geol 46 (3):250–261
Härma P, Vepsäläinen J, Hannonen T, Pyhälahti T, Kämäri J, Kallio K, Eloheimo K, Koponen S (2001) Detection of water quality using simulated satellite data and semi-empirical algorithms in Finland. Sci Total Environ 268(1–3):107–122
Hölting B, Haertle T, Hohberger K-H, Nachtigall KH, Villinger E, Weinzierl W, Wrobel J-P (1995) Konzept zur Ermittlung der Schutzfunktion der Grundwasserüberdeckung [Concepts for the investigation of the protective function of the groundwater overlying layers]. Geol Jahrb C63:5–24
Hötzl H, Delporte C, Liesch T, Malik P, Neukum C, Svasta J (2004) Risk mapping. In: Zwahlen F (ed) COST Action 620: vulnerability and risk mapping for the protection of carbonate (karst) aquifers. Final Report, Office of the Official Publications of the European Communities, Brussels, Belgium, 297 pp
Hudson SJ, Moore GF, Bale AJ, Dyer KR, Aiken J (1994) An operational approach to determining suspended sediment distributions in the Humber Estuary by airborne multi-spectral imagery. Proc Int Airborne Remote Sens Conf 3:10–20
Kim K, Ventura S (1993) Large-scale modeling of urban non-point source pollution using a geographical information system. Photogramm Eng Remote Sens 59(10):1539–1544
Koponena S, Pulliainena J, Kalliob K, Hallikainena M (2002) Lake water quality classification with airborne hyperspectral spectrometer and simulated MERIS data. Remote Sens Environ 79:51–59
Magiera P (2000) Methoden zur Abschätzung der Verschmutzungsempfindlichkeit des Grundwassers [Methods for estimating groundwater vulnerability]. Grundwasser 3:103–114
Magiera P (2002) GIS-gestützte Bewertung der Verschmutzungsempfindlichkeit des Grundwassers [GIS-based evaluation of the groundwater vulnerability]. Geologisches Jahrbuch Sonderheft, Reihe C, Heft SC 3, Schweizerbart, Stuttgart, Germany
Margane A (2002) Criteria for the preparation of groundwater vulnerability maps. Technical Report Nr. 2, Technical Cooperation Project No.: 2001.2132.7. Ministry of Water and Irrigation MWI, Amman, Federal Institute for Geosciences and Natural Resources BGR, Hannover, Germany, 80 pp
Masri M (1963) Report on the geology of the Amman, Zerqa area. Central Water Authority, Amman, pp 1–74
Mattikalli MN, Engman ET (2000) Integration of remotely sensed data into geographical information systems. In: Schultz GA, Engman TE (ed) Remote sensing in hydrology and water management. Springer, Berlin, 475 pp
Merchant JW (1994) GIS-based groundwater pollution hazard assessment: a critical review of the DRASTIC model. Photogramm Eng Remote Sens 60(9):1117–1127
Mikbel SH, Zacher W (1981) The Wadi Shueib structure in Jordan. Neues Jahrb Geol Paläontol, Monatsh 9:571–576
Ministry of Agriculture (1994) National soil map and land use project: the soils of Jordan vols 2–3, Level 2, semi-detailed studies. Hunting Technical Services Ltd. Houston, Texas

 DOI 10.1007/s10040-007-0202-0

OKI (Ohio-Kentucky-Indiana Regional Council of Governments) (1975) A method for assessing rural non point sources and its application in water quality management. WH-554, OKI, Cincinnati, OH, USA, 20 pp

Orthofer R, Shuval H, Issac J, Daoud R, Kupferberger H (2001) Developing sustainable water management in the Jordan Valley Final Report, INCO-DC Contract no. ERBIC18CT970161, EU, Brussels, 64 pp

Powell JH (1989) Stratigraphy and sedimentation of the phanerozoic rocks in central and south Jordan: part B Kurnub, Ajlun and Belqa Groups. Ammam Geol Map Div Bull 11B:127

Quennel AM (1951) The geology and mineral resources of Transjordan. Colon Geol Miner Resour 2:85–115

Ragan RM, Rogers RH (1978) Use of LANDSAT satellite remote sensing for regional environmental planning and management. XV Convention Pan American Federal of Engineering Societies, Santiago, Chile

Rosen L (1994) A study of DRASTIC methodology with emphasis on Swedish conditions. Groundwater 32(2):278–285

Salameh E (1980) The Suweilih Structure. Neues Jahrb Geol Paläontol Monatsh 11:428–438

Salameh E (1996) Water quality degradation in Jordan. Royal society for the conservation of nature. Deposit No. (1134/8/1996). Friedrich Ebert Stiftung, Bonn, Germany, 180 pp

Schecter RN (1976) Resources inventory using LANDSAT data for area wide water quality planning. Proc. Symp. on Machine Processing of Remotely Sensed Data, Laboratory of applications of remote sensing, Purdue University, West Lafayette, IN, USA

Schultz GA, Engman ET (2000) Remote sensing in hydrology and water management. Springer, Heidelberg, 483 pp

Spiteri A (2004) Data collection using remote sensing. In: Zwahlen F (ed) (2004) COST Action 620: vulnerability and risk mapping for the protection of carbonate (karst) aquifers. Final Report, Office of the Official Publications of the European Communities, Brussels, Belgium, 297 pp

Srivastava A, Tripathi NK, Gokhale KV (1997) Mapping groundwater salinity using IRS-1B LISS II data and GIS techniques. Int J Remote Sens 18(13):2853–2862

Star J, Estes J (1990) Geographic information systems: an introduction. Englewood Cliffs, New Jersey, 250 pp

Svoma J, Pysek A (1985) Photographic detection of groundwater pollution. In: Goodison BE (ed) Hydrological applications of remote sensing and remote sensing data transmission. Int Assoc Hydrol Sci Pub 145:561–567

Ta'any RAA (1992) Hydrological and hydrochemical study of the major springs in the Wadi Shueib catchment area. McS Thesis, Yarmouk University, Irbid, Jordan, 300 pp

Thiemann S, Kaufmann H (2002) Lake water quality monitoring using hyperspectral airborne data: a semiempirical multisensor and multitemporal approach for the Mecklenburg Lake District, Germany. Remote Sens Environ 81:228–237

Vrba J, Zoporozec A (eds) (1994) Guidebook on mapping groundwater vulnerability. Int Contrib Hydrogeol (IAH) 16:131

Zwahlen F (ed) (2004) COST Action 620: vulnerability and risk mapping for the protection of carbonate (karst) aquifers. Final Report, Office of the Official Publications of the European Communities, Brussels, Belgium, 297 pp

 DOI 10.1007/s10040-007-0202-0